Simulation and analysis of an x-ray-heated boron nitride foil

J. D. Bauer, C. A. Back, J. I. Castor, P. G. Dykema, B. A. Hammel, R. W. Lee, and J. K. Nash
Lawrence Livermore National Laboratory, Livermore, California 94550

J. F. Seely, U. Feldman, and C. M. Brown
Naval Research Laboratory, Washington, DC 20375
(Received 22 March 1995; revised manuscript received 18 July 1995)

We analyze an experiment performed at the Nova laser facility, at Lawrence Livermore National Laboratory, in which x rays, produced by a gold burn-through foil, heated an 1800-Å boron-nitride (BN) foil. The BN foil was not hydrodynamically tamped and therefore provides an excellent example for testing our success at modeling systems with large density and temperature gradients. A time-integrated absorption spectrum was obtained. This spectrum reveals He-like and H-like boron features, He-like nitrogen features, as well as Li-like satellites to the resonance lines for both boron and nitrogen. The ALTAIR radiation hydrodynamics code and the TOTAL line-shape code were the basic instruments used in the analysis. Simulations address the temporal evolution of the temperature and density profiles as well as the ionization balance for the x-ray driven boron nitride foil. A synthesized spectrum is compared with the experimental absorption spectrum, and particular attention is given to the Li-like satellite structure. The analysis of this seemingly simple experiment clearly reveals both current strengths and inadequacies in modeling hot dense matter.

PACS number(s): 52.70.La, 52.25.Jm, 52.25.Nr, 52.25.Dg

I. INTRODUCTION

The study of radiative properties in hot dense plasmas is a complex and important problem in high-energy density physics. Understanding the detailed manner in which energy is transported into and heats a sample requires comprehensive knowledge of atomic physics, kinetics, radiation transport, and spectral line-shape theory. Since the nature of hot dense matter is, therefore, an admixture of complex topics, each difficult in its own right, one must make recourse to critical experimental techniques to assist in developing an understanding of these plasmas. Therefore, the ability to perform accurate experiments in this regime is essential. The past has seen little substantive progress in the production of hot dense matter that could be used to disentangle the complexities of the plasma production from the underlying physical phenomena. More recently, with the advent of large high-energy lasers, the ability to produce hot dense plasmas that are amenable to detailed study has led to the possibility that we are at the starting point of a new era in studies of these plasmas. Specifically, experiments have been performed where we can measure the temperature of certain local thermodynamic equilibrium (LTE) plasmas to $\pm 2\%$ and the density to $\pm 10\%$ in regimes where the energy density is extremely high [1]. This leads us to two separate paths of attack on the problem of understanding the details of the radiative properties of hot dense matter.

First, with the techniques developed previously for single temperature and density samples, we can proceed to extend these techniques to non-LTE systems. This can be achieved by using the concepts originally developed for the use in enclosed radiation environments, i.e., hohlraums, but now can be applied to the study of the piasmas as they evolve to lower density, but with controlled, small gradients. These experiments are ongoing and diagnostics are being developed [2].

Second, one can examine samples that are not hydrodynamically tamped, and which therefore have large gradients. These plasmas will have surfaces that freely expand into the vacuum; the rarefied outer parts will likely be non-LTE owing to their low density, and increasingly so as the expansion proceeds. The requirements on the simulations and the measurements relevant to experiments with large gradients is the subject of the present work. This work will highlight the state of progress in these experiments, the level of sophistication that is required from the simulations to make critical comparisons between the experimental data and the simulated spectrum, and discuss improvements necessary in the experiments. In particular we will discuss the experimental requirements with respect to data reduction, spectral range, and resolution. We will present a study of the limitations of the simulations in regard to the initial inputs—for example, atomic data and quantitative x-ray flux information—as well as the limits of the experiment-theory comparisons. The emphasis is therefore not on how well the simulation and experiment agree but on those areas where more effort is needed.

As an overview we will be discussing an experiment in which a sample is volumetrically heated by a measured x-ray flux: a gold foil is irradiated with one beam of the Nova laser, located at Lawrence Livermore National Laboratory, and its radiation is used as an x-ray source. This source is allowed to radiatively heat a sample of material that is optically thin to the x-ray flux. A probe, or backlight, formed by a second similarly produced x-ray source,

1063-651X/95/52(6)/6736(17)/$06.00

when passed through the heated sample is used to reveal quantitative information about the ionization balance of the constituent materials. Thus, we may obtain insight into the hydrodynamic state of the material or equivalently the radiation-matter interaction. Analysis of this experiment obviously requires accurate hydrodynamics as well as radiative transfer calculations. Attempts at modeling experiments, even simple ones, strain our current abilities both from a purely theoretical perspective as well as a computational perspective.

This paper is organized in the following manner. In Sec. II the experimental arrangement and the data reduction techniques will be presented. In Sec. III the initial information required for the simulations is discussed. Here the reduction of the experimentally determined x-ray flux and the atomic physical constants are presented. In Sec. IV we present the results and discussions of the simulations. We review the plasma temperature and density obtained in the simulations, as well as the computed ionization balance, to provide better understanding of the comparison with experiment contained in Sec. V. In the comparison we contrast the synthetic and experimental spectra and provide a discussion of the satellite line strengths and finally the satellite spectra. We also describe how satellite line data of spectroscopic accuracy were sought and how these were used in the TOTAL code [3] to provide line shapes of the satellite line groups, and the results of comparing these calculations with the experimental data. Finally, in the Appendices we include the response curve for 101-5 Kodak plates and the satellite line data.

II. EXPERIMENT

The experimental configuration employed to obtain an absorption spectrum of an x-ray heated sample is shown in Fig. 1. Here we see that the basic requirements of diagnostic access, an independent x-ray heating source, and an independent x-ray uv (XUV) backlight are achieved in a simple and compact target. Further, the requirement that the heated sample be hydrodynamically isolated is satisfied by making the separation of the sample and heater 0.33 cm, and the separation of the sample and backlight 1.0 cm. References [4,5] give useful details about this experiment, about the identification of the spectral features, and especially about the methodology of extracting the sample transmission from the measurements of plate density.

Specifically, the experiment involved the irradiation of an 1800-Å-thick sample of boron nitride for approximately 1 ns by the flux produced from a 2500-Å-thick gold heater foil [4,5]. The sample consists of a thin, 0.18-μm thick free standing boron nitride foil. This foil was fabricated by vapor deposition onto a Si substrate, which was then removed by etching. It was determined that the composition was 84.6% B, 13% N, and 2.3% O, or roughly $B_{13}N_2$ [6]. The analysis also revealed a surface layer heavily (24%) contaminated with carbon, which is presumably the origin of a hot carbon feature in the spectrum that will be discussed below. The sample foil was

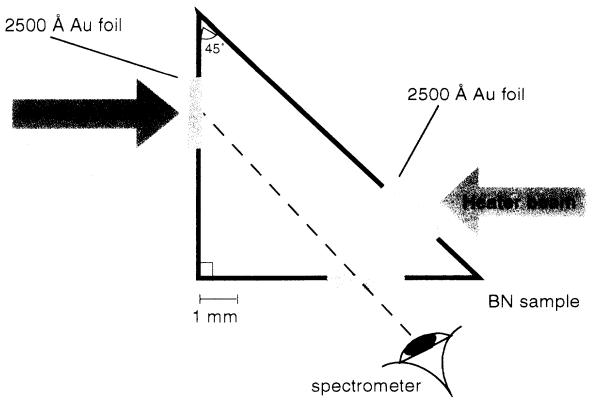

FIG. 1. The experimental arrangement. The triangular structure is a hollow copper prism into which three windows are machined where stainless steel washers are mounted. The BN sample is mounted on one of these washers, and gold foils are mounted on the other two. The beams of the Nova two-beam facility are focused on the gold foils. The spectrometer line of sight is directed through the sample foil at the backlight foil, as shown.

positioned covering just half a window in the target. In this way the spectrometer could, with one spatially resolving dimension, measure the backlight both with and without the attenuation of the $B_{13}N_2$. This simultaneous measurement is important to the quantitative analysis of the data, as will be discussed below. As discussed in Refs. [4,5], the NRL 3-m spectrograph [7], with its entrance slit, provides spatial imaging—in the direction perpendicular to the dispersion—of both the backlight foil and the sample foil.

A time-integrated absorption spectrum was obtained over the duration of the backlight, which was also approximately 1 ns in duration. The spectrum reveals prominent absorption features from B III through B V and N V through N VII. In particular the He-like and H-like Lyman series members $n = 1$ to $n = 2$–5 were observed for both atomic species (but only He-like for nitrogen) as well as Li-like satellites to the resonance lines of both elements, and He-like satellites to the H-like boron resonance line.

The K-line spectrum of B and N in the present experiment consists of the resonance lines of the H- and He-like ions, and the inner-shell 1 to n transitions of the Li- and Be-like species. The lines of H-like and He-like B and He-like N are quite saturated, and thus their strength in the absorption spectrum is sensitive to local line broadening mechanisms as much as, or more than, to the column density of the ion in question. The inner-shell $K\alpha$ and $K\beta$ of the Li-like and Be-like ions are in reality groups of satellites to the He-like resonance lines, and each group contains lines with a considerable range of strengths. This makes the measured satellite line strengths a good tool for deducing the ionization balance in the experiment, and thereby the temperature and density.

The experimental data are shown in Fig. 2. In this two-dimensional image the abscissa is in the spectral dispersion direction. Both a scale of photon energy in eV

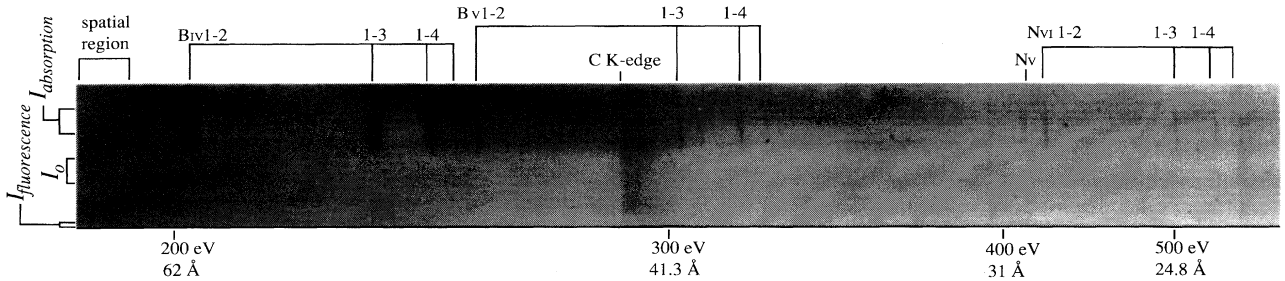

FIG. 2. The plate record obtained in the experiment. The annotations show the wavelength and photon energy scales and the areas used for the backlight and absorption spectra and the fluorescence signal estimate.

and a wavelength scale in angstroms are shown below the image. The ordinate is the spatial dimension, with the region that shows the unattenuated backlight at the lower part of the image and the attenuated spectrum at the upper part. A tiny region along the bottom edge of the film was not exposed to the backlight, and this was used to estimate the fluorescence intensity. The goal of the quantitative analysis of these experimental data is to measure the absorption spectrum resulting from a characterized backlight.

The intensity that is recorded is the integral over time of the absorption. The recorded signal for the absorption becomes

$$I(\nu)_{\text{absorption}} = \int I(\nu,t)_{\text{absorption}} dt \ , \tag{1}$$

with a similar equation for the backlight intensity I_0. With this we will find that the quantity we derive from the experiment is the normalized transmission defined as

$$T(\nu) = \frac{I(\nu)_{\text{absorption}}}{I_0(\nu)} \ . \tag{2}$$

The data reduction indicated in Eq. (2) has been carried out using the regions of the data image indicated in Fig. 2. The subtraction of the fluorescence has been accomplished and the regions of the image used to generate the backlight intensity and the absorption intensity are shown. The division indicated in Eq. (2) then yields the results shown in Fig. 3.

In Fig. 3 we see the normalized transmission plotted as a function of energy in eV. The range of the spectrum from 190 to 600 eV, covering both the boron and nitrogen K-shell regions, as well as the high resolution of the spectral features, shows the advantages of the 3-m spectrometer [5]. Several features of the reduced data are of importance to the comparison with simulation. First, the dispersion was determined by locating the strong resonance lines, fixing the wavelength, and applying the dispersion formula for the Rowland circle instrument. This provisional photon energy scale was corrected by fitting the residuals between the derived and tabulated energies of H- and He-like lines to a cubic polynomial. The final energies should be accurate to ± 0.1 eV.

Second, there are absorption features that are not due to any known transition in B or N. One is a broad absorption beginning at 287 eV. The likeliest identification is with the cold carbon K edge (284 eV), and it might come from residual carbon in the $B_{13}N_2$ target. If the carbon were to be on one of the elements of the spectrometer then the division performed should have removed the feature. A sharp line feature at 308 eV coincides with the resonance He α line of C V. The source of this absorption is surely residual carbon in the target, and the much lower ionization evident in the 287-eV feature makes it likely that the cause of the latter is carbon in some element of the spectrometer, for which the correction is incomplete. We note here that slight variations in the spatial flat fielding along the spectral direction would explain this residual absorption. Line features that are seen at 574 and 563 eV agree very well with the energies of the O VII He α line and the associated lithiumlike satellites, respectively, and could well be due to the oxygen contamination (of order 2%) in the sample foil.

III. SIMULATION AND ANALYSIS

This experiment has been analyzed using the ALTAIR code [8]. ALTAIR can operate in two modes. One mode allows us to obtain a time history of the hydrodynamics from a separate code and feed it into ALTAIR. In this mode ALTAIR solves the time-dependent radiative transfer equation using the external densities and temperatures. In the other mode, ALTAIR performs the entire time-dependent hydrodynamics and radiative transfer calculations. We have used ALTAIR in both modes. The results are consistent with each other and with the experiment.

Several items of information are needed in order to perform an ALTAIR calculation. We must know the heater and backlighter sources—we are given the experimentally determined flux at the surface of the gold foil and we need to account for the distance to the boron nitride (BN) sample in the experimental geometry. Calculations show the backlight to be somewhat significant relative to the heater—7.7%.

Measurements have been made of the rear-side flux of the gold heater foil [9], and these data are used in the simulations. In Fig. 4 we show the flux emitted from the Au foil in units of J/keV/ns into 4π versus spectral energy in eV. Each curve represents a different time, at increments of 200 ps. Details about this flux can be found in the reference. The radiation density used in the simulations is the quantity E given by $E = \Omega H/(4\pi c A_S \cos i)$, where

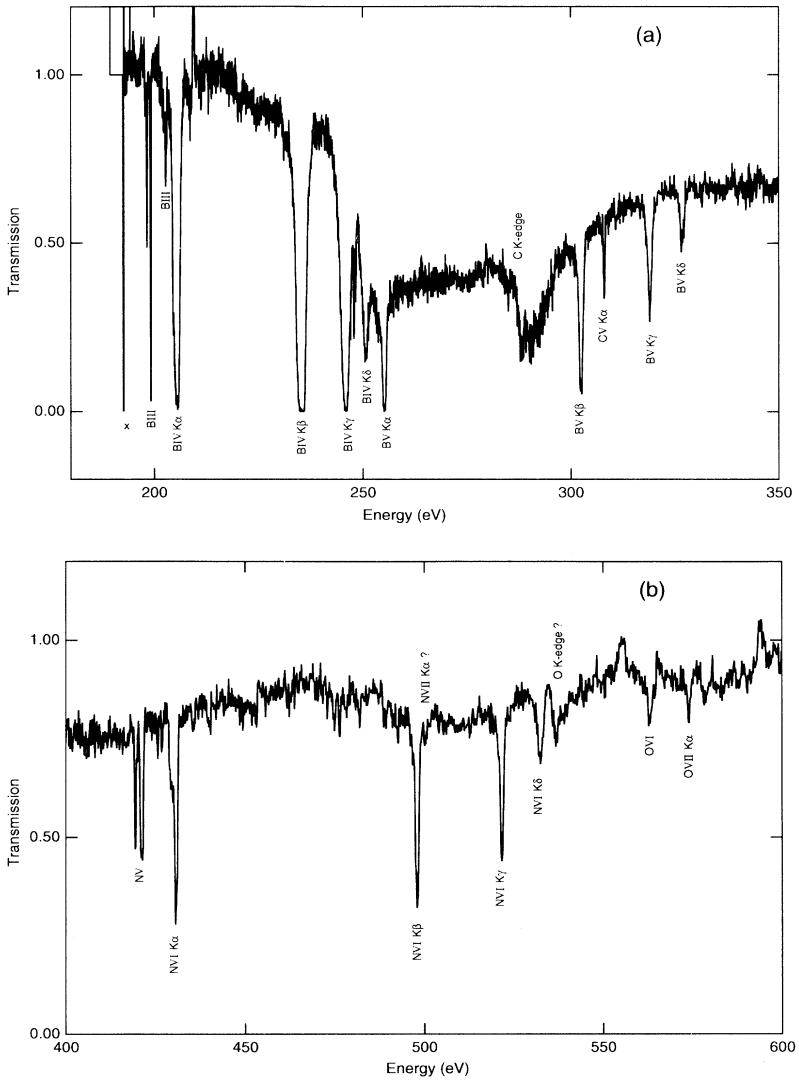

FIG. 3. The calibrated transmission spectrum obtained as described in the text. The ordinate is fractional transmission of the BN sample; the abscissa is photon energy in eV. (a) The region of the B lines. (b) The region of the N lines.

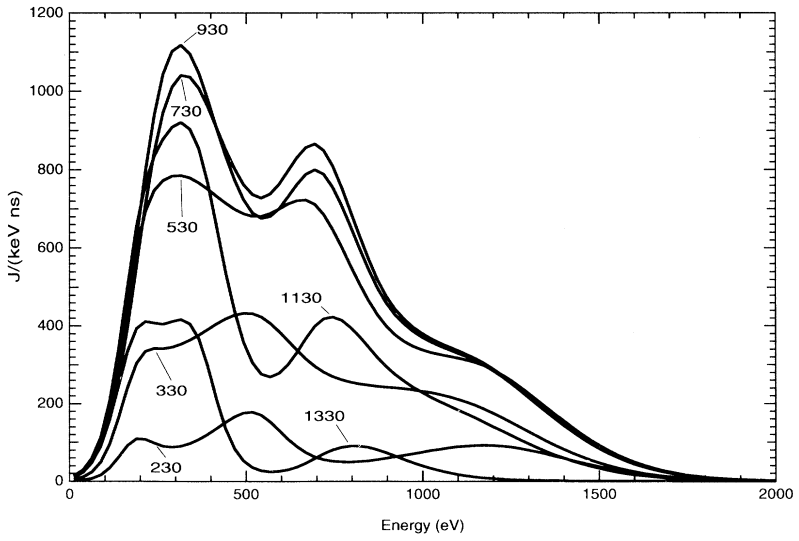

FIG. 4. Flux spectrum emitted by the 2500-Å Au foil at various times (in ps) after the beginning of the laser pulse, indicated by the labels. The ordinate is 4π times the total power per steradian emitted in the direction normal to the foil, expressed in joule keV^{-1} ns^{-1}; the abscissa is photon energy in eV.

H is the source intensity given by [9] in $\mathrm{J\,keV^{-1}\,ns^{-1}}$ into 4π, Ω is the heater solid angle at the sample (we find 0.21), A_S is the heater foil area [$(1500\,\mu\mathrm{m})^2$], and i is the inclination of the source foil to the line of sight in the calibration experiment (33°).

After an interval of about two years, the measurements of Ref. [9] were repeated [10]. In temporal and spectral characteristics the previous measurements were confirmed, but an absolute flux level 1.5 times higher was found. In the simulations to be discussed below we took the fluxes of Ref. [9] as the nominal ones, but we applied a multiplying factor to them while keeping the same spectral shape and time evolution. Our calculations with a factor of 1.5 are motivated by Ref. [10].

We also need to provide ALTAIR with atomic data. ALTAIR contains no built-in information of this kind so external atomic models are necessary. The tools we have used for this are the packages VAPP and AEOS constructed for the Cray computers [11]. VAPP is a shell that runs the MCDF code [12] to perform relativistic atomic structure calculations in the Dirac-Fock approximation. In this instance VAPP generated the energy levels and oscillator strengths. Photoionization data are calculated using an independent electron model based on a Dirac-Hartree-Slater average-atom calculation [13]. The important autoionizing doubly excited states were assigned autoionization decay rates computed with a code AUTOVAPP based on the method of Ref. [14]. These data are assembled by the AEOS code—which further supplied collisional ionization cross sections—to produce large text files, called "models," that contain all the required data in readable form. The present ALTAIR calculations used models named "d05a3" and "d07a3" for boron and nitrogen, respectively. Before the models were used, slight adjustments were made to some of the energy levels for which accurate experimental data exists, such as for the He-like species.

The boron and the nitrogen models were constructed to span the range of ion species between beryllium-like—the most recombined—and fully stripped for both boron and nitrogen, i.e., B II–B VI and N IV–N VIII. Each ionic stage contains the levels of principal quantum number $n = 1$ to $n = 5$, including core-excited levels, with full detail in n, ℓ, j and the fine structure. In total the model contains 908 levels, 344 levels for boron and 564 for nitrogen.

All the atomic data are in the isolated-atom approximation; no corrections are included for plasma effects such as continuum lowering. Indeed, we lack a theoretical framework for non-LTE calculations in the presence of such effects. Certain of our results should be robust with respect to the plasma effects, such as the ionization balance, while we will note this deficiency in the cases in which it is a serious lack, such as the shape of the Rydberg confluence region of the spectrum.

The initial sample thickness and density are appropriately set, and the chemical composition of the sample is inserted ($B_{13}N_2$). We have ignored the small oxygen contamination, except to note that is is probably responsible for the He-like and Li-like O $K\alpha$ features that are seen in the experimental spectrum.

The radiative-transfer calculation included approximately 350 explicit line transitions—those lines for which radiative transfer is frequency-by-frequency, as opposed to an optically thin approximation. The experimental range of interest is 180–610 eV. This range and the optical depth of each transition provided a guide to select the transitions to be given detailed radiative-transfer treatment. Essentially, in the energy range of interest, lines with an optical depth > 0.01 were "turned on"—designated for equivalent two-level-atom treatment—for the transfer calculation [8]. This criterion was varied to ensure the results were not greatly influenced by our choice of transitions.

The simulation proceeds as follows: initially one edge of the BN slab is placed at $z = 0$ and the other at $z = 1800$ Å. The radiation impinges on the sample at the $z = 0$ boundary, which is referred to as the left edge or the front of the slab. A combined hydrodynamics and radiative-transfer calculation is then performed. A time of 230 ps, for historical reasons, corresponds to the origin of time, i.e., the time when the heater is turned on. Thus the Nova heater pulse lasts nominally from $t = 0.23$ ns to $t = 1.23$ ns, and the backlighter pulse, delayed by 0.7 ns, lasts from $t = 0.93$ ns to $t = 1.93$ ns. Both gold foils continue to glow somewhat after the laser pulse is off, of course. For computational convenience the transmission is calculated by applying a very weak "probe" flux, proportional to the backlight flux, to the *right* (spectrometer) side of the slab. This probe flux has the same temporal and spectral characteristics as the actual backlight, but is several orders of magnitude weaker so as not to perturb the calculation. Both the incident probe flux and the portion of it that emerges from the *left* (heater foil) side of the sample are integrated over time, corresponding to the time integration that the plate performs. During the course of the simulation, roughly 2 ns, the BN foil expands from 0.18 μm to approximately 600 μm.

Three different ALTAIR calculations will be described: "bnfs", which is a calculation using density and temperature results from LASNEX [26], fed into ALTAIR; "bnla," a calculation using ALTAIR's hydrodynamics and energy balance calculation, and "bnlb," which also used ALTAIR's hydro and energy balance. For "bnfs" and "bnla" the nominal intensity of the heating source from Ref. [9] was multiplied by 1.5×, while for "bnlb" the factor was 2×. The factor 1.5×, we recall, brings the fluxes of Ref. [9] into approximate agreement with those of Ref. [10]. We have also used the factor 2.0× because, as we shall see below, the predicted degree of ionization is still somewhat too low when the factor 1.5× is employed. This disagreement is ameliorated but persists even with the factor 2.0. These three calculations show significant differences and are discussed in more detail later on in the paper.

Figures 5 and 6 present snapshots of the electron temperature and electron density from calculation "bnla" as a function of coordinate in the slab at times representing the beginning, middle, and end of the backlight pulse. The temperature profile becomes asymmetric with the back end cooler than the front and a maximum toward the forward central region. The electron density only be-

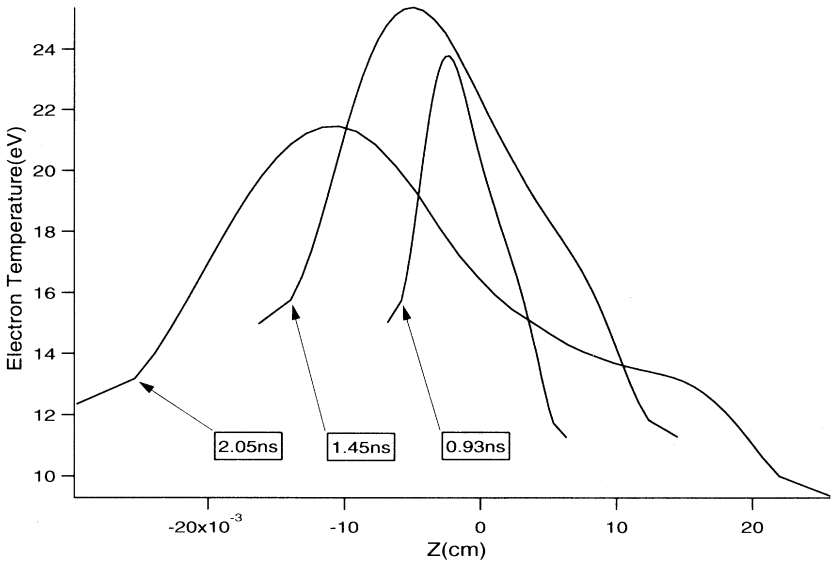

FIG. 5. Electron temperature vs distance normal to the BN foil for three times during the expansion.

comes slightly asymmetric throughout this interval. The BN attains a maximum temperature of about 25 eV near the center of the expanded slab at a time about half way through the backlight interval. The electron density at the same time, in this region, is about 7×10^{20} cm^{-3}.

The LASNEX calculation of temperature and density produces a temperature that is significantly lower than ALTAIR's on the back side of the slab. We have investigated the reason for this, and find that the heating of the material is dominated by radiation at a frequency of a few hundred eV, and that with ALTAIR there is appreciably less attenuation of this radiation by bound-free absorption than LASNEX calculates. The detailed atomic model used in ALTAIR makes its photoabsorption calculation much more accurate than with the very simplified model in LASNEX.

The effect of uncertainty in the photoionization cross sections has been investigated as well. A 25% increase in the ground-state photoionization cross sections produces about a 4% rise in peak temperature in the slab at a typical time. The ionization balance is affected in that the most abundant ion species, He-like boron and nitrogen, change by less than 10%. The Li-like ions of boron and nitrogen similarly change by less than 10%. There is a substantial change in the H-like and bare components; however, their actual abundances are minute and so this change does not significantly alter the previous results. The interpretation of these changes is simple: The increased photoionization cross sections resulted in a small increase in deposited energy, and therefore in the temperature of the slab. For most of the ions, which are close to LTE, the abundances track the temperature, and therefore modest increases in ionization are seen. The hydrogen-like and bare ions, however, are out of LTE, and their abundances relative to the next lower ion are directly proportional to the photoabsorption rate, and therefore to the subject cross sections. The arbitrary change of 25% is likely to be an upper limit to the actual uncertainty, and therefore the photoionization cross sections are probably not a major source of error in the results to be discussed below.

Figure 7 shows the boron ion fraction as a function

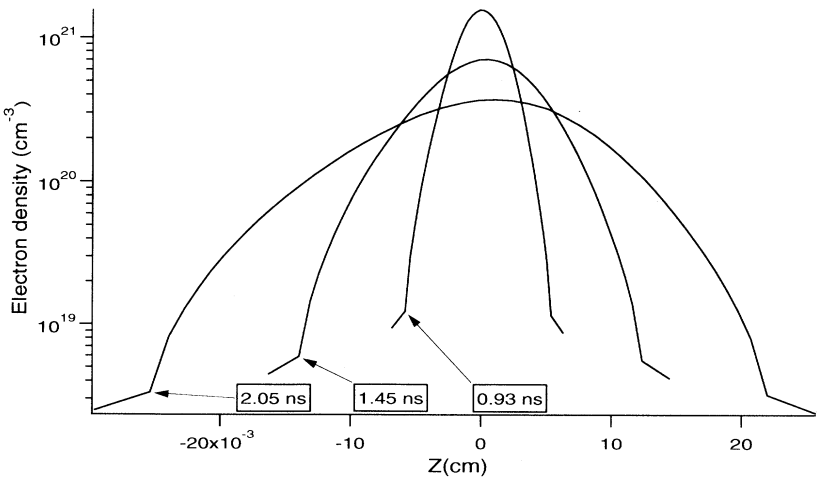

FIG. 6. Same as Fig. 5, but for electron density.

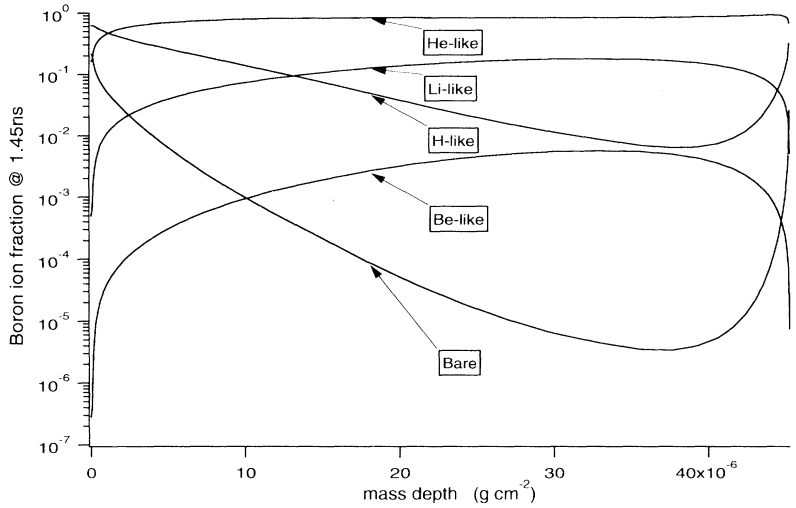

FIG. 7. Fractional abundances of boron ions at the peak of the backlight in time.

of depth, in terms of areal density, in the slab at a time half way into the backlight pulse, 1.45 ns. Conditions at this time are fairly representative for the major contributors to the time-integrated absorption spectrum. In the low-density forward region, the H, He, and fully stripped components are dominant with hydrogenlike boron being most abundant. In the high-density middle region, the populations cross over with hydrogenlike and fully stripped boron considerably dropping off and He-like dominant. The far end of the slab shows a reemergence of the hydrogenlike and fully stripped boron as the density drops; however, the He-like is dominant in this region as well.

The nitrogen abundances are shown in Fig. 8. The behavior of the hydrogenlike and bare nitrogen, being greatly influenced by the density changes throughout the slab, is similar to the comparable ion species for boron. The He-like nitrogen fraction is greatest in the forward region and shares that distinction with the Li-like ion in the far end of the slab. The Li-like and berylliumlike nitrogen absorption features are visible in the calculation but not to the same extent in the experiment. In fact the Be-like appears to be absent in the experiment. The presence of Be-like and Li-like nitrogen in the far end of the slab is quite sensitive to the temperature in that region and simulations show a few electronvolt difference in the temperature makes a profound difference in the magnitude of those spectral features. This point will be discussed in Secs.V A and V B.

A sample of the temporal variation of the ionization balance is presented in Fig. 9, which depicts the ionization of nitrogen at the face of the foil toward the heater source. The rate of change of the ionization slows considerably after about 1.2 ns. This can be understood by noticing that the electron-ion recombination times are of the order of 1 ns, and are especially long at late time in the rarefied outer layers. This "freezing-in" effect that decompression has on the ionization is less noticeable at the center of the slab. Another effect that can be observed in the bare and H-like ions is that the abundances of these species at the center of the slab drop when, first, the heater flux disappears, then even more when the backlight flux also drops. These ions are produced largely by photoionization rather than collisionally.

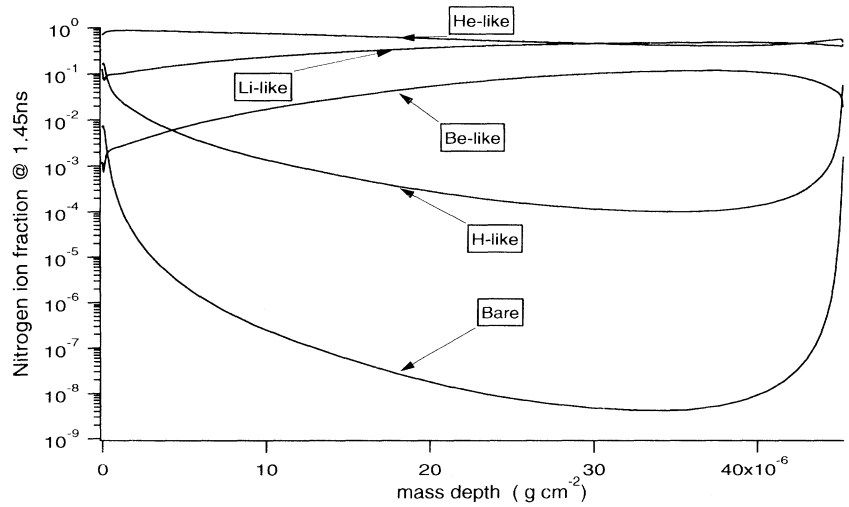

FIG. 8. Same as Fig. 7 for nitrogen ions.

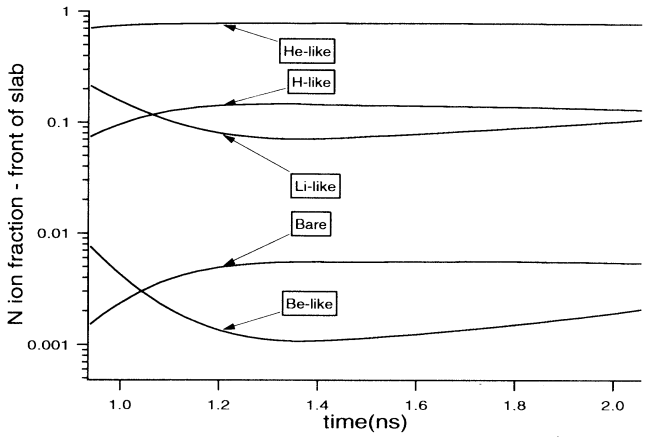

FIG. 9. The time history of the fractional abundances of the ions of nitrogen at the front side of the foil—the side facing the heater.

Throughout the slab the He-like and H-like populations of both boron and nitrogen are dominated by the ground state. This is not true, however, for the Be-like and Li-like sequences. These ions have several low-lying terms of the ground configuration that are metastable and are well populated. Excited-state configurations lying $\gtrsim 200$ eV above the ground state in the Be-like and Li-like species are populated as a result of the driving radiation. The H-like and fully stripped nitrogen are severely overpopulated relative to what one would expect from LTE considerations.

IV. ABSORPTION SPECTRUM

ALTAIR currently does not incorporate the effects of ionization level depression or a thorough treatment of line broadening due to Stark effects. How this affects the agreement between ALTAIR and the experimental spectrum is easily seen in Fig. 10: The sharp photoionization edge in the calculation at 259 eV (the ionization potential of B IV) is missing in the experimental spectrum, where the continuum extends down to about 250 eV; at this energy the continuous absorption appears to become weaker, and it is overlain at this energy with a weakened B IV He δ ($n = 1$ to $n = 5$) line. The precise shape of the absorption spectrum in this region clearly conveys some valuable information about the process of "continuum lowering." The line at 255 eV is Lyman-α of B V, which, since it belongs to the higher ion, is not affected by continuum lowering in this region.

The experimental and calculated absorption spectra in the nitrogen region are shown in Fig. 11. There is good general agreement between the calculation and the experiment on the strength and shape of the continuous absorption for both boron and nitrogen. Unfortunately, the systematic errors of the plate calibration introduce features in this continuous absorption, especially from the cold-C K edge at 284 eV up to the limit of Fig. 10 at 350 eV. These mask somewhat the gentle frequency variation of the actual absorption.

There are several gross features of the boron and nitrogen line spectra that deserve comment. In particular the experiment contains absorption features due to He-like boron from the ground state through $n = 5$, and H-like boron features from the ground state through $n = 5$. Two narrow absorption features in the blue wing of the boron He γ line are due to the He-like satellite transitions $1s2p\,^3P^o$–$2p^2\,^3P$ and $1s2s\,^3S$–$2s2p\,^3P^o$. Lithiumlike absorption features are present for boron as well. The features visible for nitrogen include the absorption due to He-like nitrogen from $n = 1$ through $n = 6$, and a number of Li-like satellite lines. The hydrogenlike nitrogen $n = 1$ to $n = 2$ transition at 500.5 eV is calculated to have a detectable strength, and possibly is present in the experimental spectrum. The ionization balance between He-like and H-like N is quite far from LTE, which makes the strength of the H-like line all the more interesting—the H to He ratio is directly related to the photoionizing flux, and not especially sensitive to the plasma tempera-

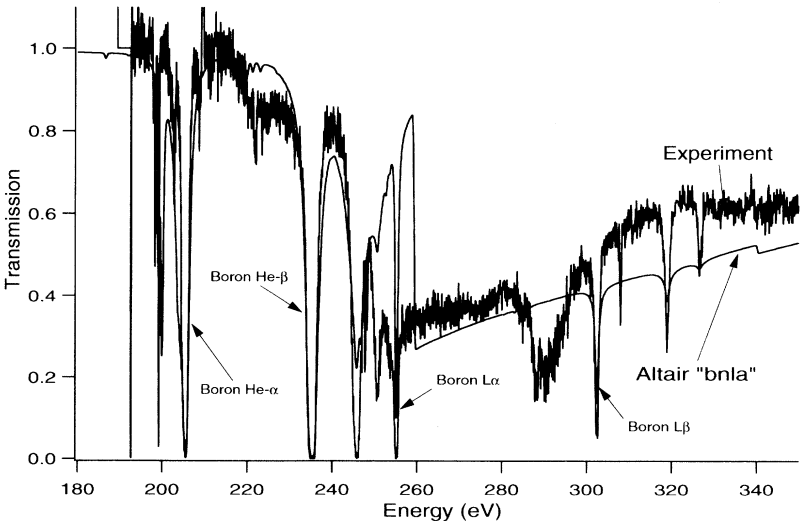

FIG. 10. Comparison of the experimental and computed spectral transmissions for the BN slab, averaged over the duration of the backlight, in the spectral region of the boron lines. The ALTAIR calculation "bnla" is shown. A few of the strong lines are identified.

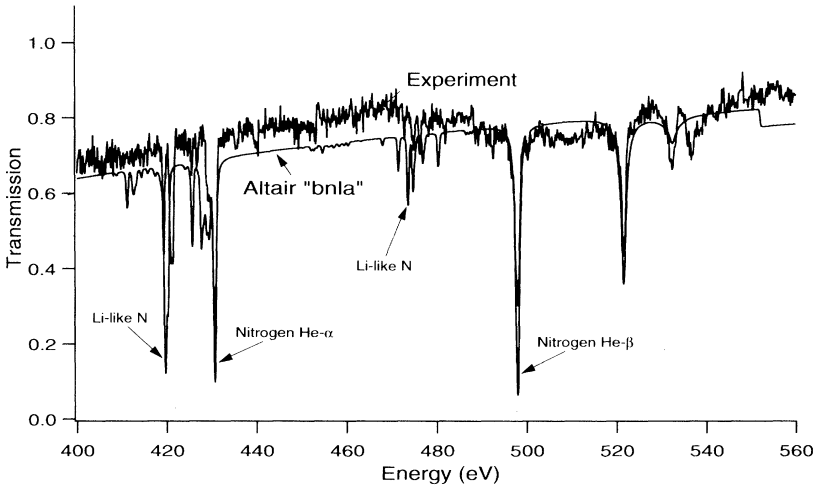

FIG. 11. Same as Fig. 10, but for the nitrogen line spectral region.

ture. We discuss below how the experimental upper limit to the strength of the H line constrains the possible values of the heater flux.

The following sections deal with the details of the satellite line spectra.

V. THE SATELLITE LINES

The ALTAIR simulations of this experiment have been based on particular atomic models for boron and nitrogen. The atomic structure input for these models came from VAPP calculations, that is, from multiconfiguration Dirac-Fock calculations using the MCDF code [12]. In Li-like nitrogen the configurations $1s2\ell2\ell'$ produce states excited about 400 eV from the ground states $1s^22\ell$. The MCDF calculations of the excitation energies have errors of order 2 eV. One or two of these could be corrected using experimental data (from Ref. [15]); most could not. The adopted models included these corrections when possible.

The success of this approach can be judged from Fig. 12, in which the time-averaged sample transmission from the ALTAIR calculation "bnla" is compared with the experiment in the region of the $1s2\ell2\ell'$ satellites of He-like N 1^1S-2^1P. Both the experimental data and the calculation have been smoothed to make the resolution similar. It is clear that the experimental spectrum does show some Li-like satellites, which produce the features near 420 eV and 426–427 eV, but that the computed line positions are in error by 1 V or more; this is sufficient to make identifying the experimental features difficult.

The disagreement in Fig. 12 is the motivation for seeking atomic structure calculations for the Li-like and Be-like ions that will give spectroscopically accurate line positions for the satellites. This search is described in Appendix B.

A. Calculations of satellite line strengths

The computer code TOTAL computes shapes of line clusters according to the model of quasistatic ion broadening and electron broadening in the impact approximation [3]. The energy levels to be considered are divided into a lower and an upper manifold, and the transitions between the two manifolds form the line cluster of interest. The dipole matrix elements connecting states within one of the two manifolds are used in forming the interaction potential that is responsible for the line broadening; the dipole matrix elements connecting a state of one manifold with a state of the other manifold give the strengths of the spectral lines of interest. Both sets of matrix elements come in the present case from MCDF, and are input into TOTAL. The energy levels themselves are also input. The output is a line-shape function that is normalized to the total line strength S of the cluster.

For the Li-like and Be-like ions the absorption occurs

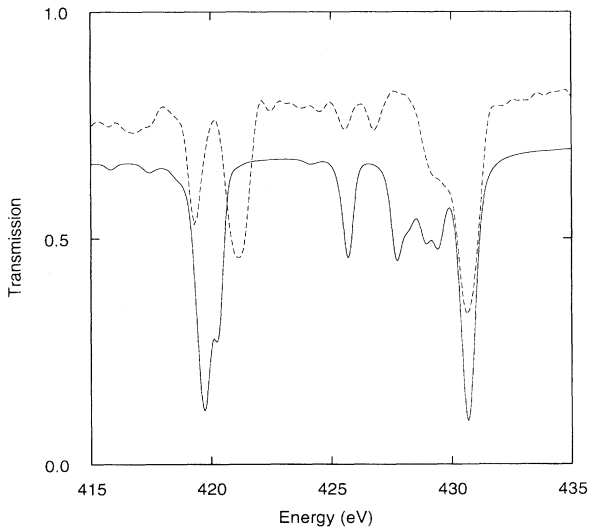

FIG. 12. Spectral transmission of the BN sample averaged over the 1-ns duration of the backlight pulse. Solid: ALTAIR simulation "bnla," smoothed 36 times to match the experimental resolution; dashed: the experimental data, smoothed 3 times to reduce the noise level. The line at 430.7 eV is the resonance line of He-like N (N VI). The other line features that are visible are due to Li-like N (N V).

from more than one lower level, although all of these are at low excitation energy and are likely to be populated closely in accordance with Boltzmann's law. To allow for this, we have added a feature to TOTAL that permits setting the lower-level population to the statistical weight of the level multiplied by $\exp(-E_{ex}/kT)$, where E_{ex} is the excitation energy of the level above the ground state. When this is invoked, the output line-shape function can be multiplied by $N(\text{ion})/Z$, where $N(\text{ion})$ is the total ion population and Z is the LTE ion partition function, to give a line-shape function correctly normalized to $\Sigma NS/g$.

For the total calculations to be discussed here the temperature has been taken to be 20 eV, and the electron density to be $4.8\times10^{20}\,\text{cm}^{-3}$. These are reasonable mean values for the conditions at 1.43 eV ns, the middle of the backlight pulse. The sensitivity to these numbers is not great, since it enters only through the Boltzmann factor used to find the populations of excited lower levels, and the collisional linewidths. The energy level data we use are discussed in Appendix B.

If the experimental configuration is approximated as a homogeneous slab of material, then the line-shape function can be transformed into the optical depth, τ_ν. For a line arising from a transition $\ell \rightarrow u$, for which the total column density through the slab of atoms in the state ℓ is N_ℓ, the optical depth is

$$\tau_\nu = \frac{\pi e^2}{mc} N_\ell f_{\ell u} \phi(\nu) \ ,$$

where $\phi(\nu)$ is the shape function for this single line, normalized over frequency. Putting in the relation between oscillator strength and line strength and changing ϕ to the energy scale in eV leads to

$$\tau_\nu = \frac{\pi e^2}{mc} N_\ell \frac{S[\Delta E(\text{Ryd})]}{3g_\ell} \frac{dE}{d\nu} \phi(E) \ .$$

The line-shape function computed by TOTAL, assuming LTE is valid, is the sum of $N_\ell(S/g_\ell)\phi(E)$ over all the lines, in units of N/Z for the ion. Thus τ_ν is obtained from this shape function by multiplying it by the (approximately constant) factor $(\pi e^2/mc)[\Delta E(\text{Ryd})/3](dE/d\nu)[N(\text{ion})/Z(\text{ion})]$. Since the total column density of the element in question (N or B) is known from the setup of the experiment, this multiplicative factor is known just in terms of the column-average ion fraction $f(\text{ion})$ and the easily calculated partition function.

The lines in the synthetic spectrum computed by TOTAL appear much more saturated than those in the experimental spectrum. In fact, nearly all the lines that are measured *are* saturated, which would be evident if the effective experimental resolving power were of order 4000 rather than 1000. The convolution with the spectral response function broadens the lines quite substantially and correspondingly reduces the depth of absorption. The reason that the effective resolving power in this spectrum is only 1000, not 3000 as implied by the spectrograph design and which has been obtained on other occasions, is not clear. We believe that the TOTAL calculations of the Li-like N satellites account for all the significant sources of intrinsic broadening (Doppler, Stark), yet the TOTAL synthetic spectrum must be convolved with a Gaussian full width at half maximum (FWHM) of 0.5 eV in order to resemble the experimental spectrum; the lines in the unconvolved synthetic spectrum have FWHM greater than or equal to 0.1 eV. A FWHM of 0.5 eV corresponds to a resolving power of 800. Furthermore, the ALTAIR (and OPAL, cf. the Acknowledgments) simulations must be smoothed with a Gaussian of FWHM of 0.4 eV to compare with the experimental spectrum. A possible source of broadening not included in the synthetic spectra is the gradient of the bulk fluid velocity along the spectrometer line of sight. However, 75% of the material has a bulk velocity less in absolute value than $7.8\times10^6\,\text{cm s}^{-1}$, corresponding to a bulk Doppler shift of ±0.11 eV. (A very small fraction of the material, at the edges of the sample, has a much higher velocity, giving a shift as great as 0.3 eV, and thus contributing to the line wings.) Therefore the cause of the 0.4–0.5-eV linewidth—corresponding to $\lambda/\Delta\lambda \approx 1000$—is not understood at present.

We believe that a useful way of analyzing the experimental data is to use the measurements of the strengths of individual lines in conjunction with the TOTAL calculations to derive values of, or limits to, the ion fractions for the various species, then use these empirical ionization data to compare with non-LTE or LTE models. To the extent that LTE is applicable, the average electron temperature of the plasma is constrained directly.

A good way to fit the measured and computed line strengths is in terms of their equivalent widths: for each line, a pass band is defined that comfortably includes it, and $\int d\nu(1-f_\nu/f_0)$ is formed over this band, where f_ν is the actual flux at frequency ν and f_0 is the local continuum flux level. For consistency, the same band is used for both the experimental and the computed spectra. One advantage of equivalent widths is that they are quite insensitive to the degradation of spectral resolution introduced by the spectrometer, the plate, etc., provided that the integration is over a wide enough band compared with the resolution element. The computed equivalent widths for the Li-like N satellites, grouped into five bands, are shown in Fig. 13. (The nomenclature of the Li-like satellites follows Ref. [16]; see also Table III.) The five bands are 400–401 eV for *op*, 418.5–420 eV for $jk\ell$, 420–422 eV for $abcd+qr$, 424.8–426 eV for *st*, and 426–427.3 eV for *mn*. Similar data were computed for Be-like N satellites in six energy bands, and for the Lyman-α lines of H- and He-like N. The analysis has not been extended to the B lines.

The measured equivalent widths just described are listed in Table I. In each case a 2σ uncertainty is attached to the value, based on the dispersion in equivalent widths computed for nearby apparently line-free bands of equal width to the one containing the line. For the lines that could not be identified in the experimental spectrum at all, such as the Be-like N satellites, this dispersion is used to set a 2σ upper limit to the true equivalent width. The TOTAL calculations, based on $T_e = 20$ eV and $N_e = 4.8\times10^{20}\,\text{cm}^{-3}$, are combined with the computed

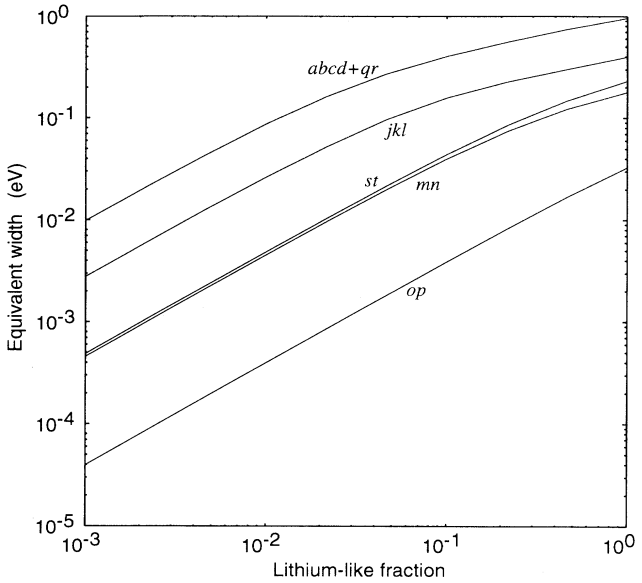

FIG. 13. Computed equivalent widths in eV of Li-like N satellites vs ion fraction, based on TOTAL line shapes for $T_e = 20\,\text{eV}$ and $N_e = 4.8 \times 10^{20}\,\text{cm}^{-3}$. The curve labels indicate the line designations in Gabriel's notation.

partition functions $Z_{\text{H}} = 2.0$, $Z_{\text{He}} = 1.0$, $Z_{\text{Li}} = 7.91$, $Z_{\text{Be}} = 36.58$ for nitrogen, and the experimental total nitrogen column density 3.20×10^{17} cm^{-3}, to produce computed equivalent widths as a function of f(ion), as in Fig. 13. These curves allow a confidence interval for f(ion) to be derived from each measured line, and these are also given in Table I. The Be-like group F is blended with Li-like *jkl*, and so no limit could be derived for this group.

The uncertainties shown for the equivalent widths in Table I represent only the random errors associated with emulsion noise and photon statistics; not included is any estimate of systematic errors that may come from the background subtraction (from diffuse emission and other scattered light and from plate fog) or from the process of division by the backlight spectrum. We are unable to quantify these, but they are no doubt appreciable. The derived values of f(ion) also have an uncertainty associated with the arbitrary choice $T_e = 20\,\text{eV}$. In fact, the TOTAL line shape and the partition function both have a moderate dependence on temperature, although these tend to cancel each other in deriving f(ion). The strength of this dependence is between $\sim T_e^{1/2}$ and $\sim T_e$. A 25% error in T_e thus causes an error in f(ion) that is probably less than 25%.

The low equivalent width of the He-like resonance line at 430.70 eV, and the corresponding low f_{He}, are causes for concern. The value $f_{\text{He}} = 0.1$ is simply not plausible. The experimental line profile is depressed only to 0.3 of the continuum, not to a few percent or less, as might be expected. The same is true of the other strong lines in the 400–500-eV region. It suggests that perhaps there is an uncorrected background that is making the absorption lines appear weaker than they should. This produces a large error in finding f(ion) from a strong line. The error is less serious for less saturated lines, but this uncertainty should be kept in mind.

B. Interpretation of the N ionization results

The results for f(ion) in Table I are summarized in Table II. The Li-line results combine to give a 90% confidence interval for f_{Li} based on a t statistic for a sample size of 4. The limit for f_{Be} given by line B is so much tighter than for the other lines that it becomes the overall limit. The limit for the H-like fraction is given, but no result is given for He-like, because of the obvious problem with that line.

Also given in Table II are the ALTAIR column-average ionization fractions at the time 1.43 ns that is half way through the backlight pulse. Three ALTAIR calculations are shown: "bnfs," "bnla," and "bnlb."

The H-like fraction is primarily sensitive to the intensity of the heater source, since the H/He balance and the bare/H balance are out of LTE and are governed by photoionization and radiative recombination, unlike the less ionized species. Thus we see that the H-He ratio tracks the source multiplier, and has 1.8× the value for "bnlb" that it has for "bnla." The equilibrium of Li-

TABLE I. Measured equivalent widths of N lines and derived ion fractions.

Line	Bandwidth	Equivalent width (eV)	Ion	f(ion)
H $L\alpha$	499.5–501.5	< 0.059	H	$< 3.2 \times 10^{-3}$
He $L\alpha$	2(430.7–433.5)	0.61 ± 0.031	He	$0.105^{+0.014}_{-0.011}$
op	400–401	< 0.05	Li	≤ 1
jkl	418.5–420	0.203 ± 0.084	Li	$0.177^{+0.240}_{-0.111}$
abcd + *qr*	420–422	0.422 ± 0.10	Li	$0.114^{+0.075}_{-0.047}$
st	424.8–426	0.046 ± 0.039	Li	$0.106^{+0.112}_{-0.091}$
mn	426–427.3	0.076 ± 0.056	Li	$0.227^{+0.329}_{-0.180}$
A	410–411.9	< 0.07	Be	< 0.112
B	411.9–413.6	< 0.06	Be	< 0.024
C	413.6–415.2	< 0.06	Be	< 0.086
D	415.2–416.6	< 0.06	Be	< 0.362
E	416.6–418.8	< 0.08	Be	< 0.330
F	418.8–420.6		Be	

TABLE II. N ionization fraction comparison.

	expt.	ALTAIR—1.43 ns		
		bnfs	bnla	bnlb
$f_{\rm H}$	< 0.0032	0.003	0.0028	0.0063
$f_{\rm He}$		0.449	0.571	0.729
$f_{\rm Li}$	0.121 ± 0.037	0.392	0.363	0.243
$f_{\rm Be}$	< 0.024	0.156	0.064	0.021

like with He-like, and of Be-like with Li-like are close to LTE, and these ratios are mainly sensitive to temperature. The changes of $f_{\rm Li}$, and especially of $f_{\rm Be}$, in the sequence bnfs→bnla→bnlb reflect the differences in the temperature structures. The "bnfs" calculation, which has the temperature computed by LASNEX, is generally the coolest, and also shows a marked tendency to be cooler on the back than on the front. The other two calculations, for which ALTAIR computed the temperature itself, are both hotter than "bnfs." For these calculations the front-to-back asymmetry is about 30%, rather than the factor of two found in "bnfs."

It is interesting to find the ranges of electron temperature that are consistent with the empirical ionization fractions on the assumption of LTE. We let the electron density be fixed at 4.8×10^{20}, the column-average value at 1.43 ns. The Be-like constraint $f_{\rm Be} < 0.024$ implies $T_e > 24$ eV. The confidence interval 0.084–0.158 for $f_{\rm Li}$ corresponds to $T_e = 29$–37 eV. Since the temperatures at 1.43 ns in all three ALTAIR simulations are confined to the range 13–28 eV, this indicates that all our hydro and energy balance calculations may be giving too low values of the electron temperature. The favored $f_{\rm Li} = 0.121$ corresponds to $T_e = 32$ eV, hotter than any calculation we have done. Increasing the heater flux multiplier sufficiently to produce this temperature will certainly violate the upper limit on the H-like fraction, besides implying a very large error in the heater flux determination itself. It remains a mystery why the experimental temperature should be so high.

C. He-like boron satellites

The experimental spectrum contains noticeable absorption features at 197.83, 198.28, 199.21, and 202.74 eV, which we identify with the Li-like boron satellite lines. We have not yet analyzed these in the manner of Sec. V A above, owing to the difficulty of finding a spectroscopically accurate set of energy levels for the doubly excited states. The line(s) at 248 eV, turn out to be the He-like satellites to the boron Lyman-α line. The line positions in the d05a3 model, generated with VAPP, are off by about 1 eV, but the wavelengths given by Vainshtein and Safronova [17] are a good deal more accurate, and allow the identifications to be made.

These lines have considerable interest, since their lower-level excitation energy is 203 eV, and thus their strengths are quite sensitive to electron temperature, provided these levels are in LTE, which the ALTAIR calculations indicate to be approximately correct—but see below. The two features are identified as $1s2p\,^3P^o$–$2p^2\,^3P$ at 247.82 eV (exp), with an equivalent width of 0.127 eV, and $1s2s\,^3S$-$2s2p\,^3P^o$ at 248.28 eV, with an equivalent width of 0.085 eV. (The equivalent widths are calculated using the wing of the He γ line as the local continuum.) The strength of the first line is turned into a temperature in the following way: The ALTAIR calculation "bnlb" gives a Doppler width of 0.0177 eV and a Voigt parameter $a = 1.34$, for the middle of the backlight pulse, and averaged through the slab weighted by the lower-level population. The He-like boron ground-state column density at this time is $1.48 \times 10^{18}\,{\rm cm}^{-2}$. The equivalent width indicates a line-center optical depth of 2.25, using an analytic curve of growth. From this optical depth, the Voigt parameter and Doppler width, the He-like boron column density and the oscillator strength, a Boltzmann exponential factor of 0.000 589 is found, which gives an excitation temperature of 27.3 eV. This is not quite as high as the temperature (32 eV) suggested by the N ionization balance, but still higher than the models predict. The equivalent width of the weaker line, $1s2s\,^3S$-$2s2p\,^3P^o$, is 0.67 times that of the stronger one, giving an optical depth 0.56 times as large. This compares well to the ratio of gf values, 0.50.

When the ALTAIR calculations "bnla" and "bnlb" are examined more closely, it is found that the populations of $1s2s\,^3S$ and $1s2p\,^3P^o$ are not *quite* in LTE: The column densities for these states at $t = 1.43$ ns are enhanced relative to LTE by modest factors—1.84 for "bnla" and 1.46 for "bnlb". The corresponding average excitation temperatures are 24.6 eV for "bnla" and 27.1 eV for "bnlb;" the averages of the actual electron temperature are 21.9 eV and 25.2 eV, respectively. Thus the NLTE effect of photopumping and radiative recombination feeding the $1s2\ell$ states makes the excitation temperature about 2 eV higher than the actual electron temperature. This is still a small fraction of the discrepancy between the empirical temperature and the predicted temperature with the nominal x-ray drive. We do note that "bnlb," with twice the nominal drive, does give just about the right excitation of the $1s2\ell$ states to explain the He-like satellites.

VI. DISCUSSION AND CONCLUSIONS

The BN experiment and its subsequent analysis bring to light important considerations concerning the design and implementation of future experiments. As mentioned in the Introduction this is the second of the two separate paths of attack on the problem of understanding the details of the radiative properties of hot dense matter; in this path we explore untamped samples that have large gradients. Since this is the goal we will separate our discussion into two parts. We will discuss deficiencies in the experimental design that come to light after rigorous data reduction and comparisons. We will discuss next those aspects of the theoretical modeling that are shown to be deficient.

A. Experimental design

In the present experiment we observe the utility of an instrument that has both broad spectral range and high

resolution. We were able to measure the relevant K-shell spectra of B and N at the same time with one dimension of spatial information. However, with these advantages came difficulties. The data reduction, for example, is fraught with procedural problems owing to the low throughput of the instrument: we have difficulty in finding the fluorescence level. The fluorescence contributes as much as some tens of percent of the total exposure on the plate, and so this must be accurately removed in order to obtain a resulting transmission that is valid to a few percent. The fact that the fluorescence varies in both the spatial and spectral directions is a major limiting factor in achieving this. As a result, the zero-intensity level is more uncertain than we would wish, with the paradoxical consequence that the strongest absorption features are poorly measured.

It is furthermore quite clear from the image that the backlight varies in the spatial dimension, that is in the vertical direction in Fig. 2. The model of backlight variation we have been obliged to use for our flat fielding (division by the backlight to obtain the true normalized transmission) is similar to that used for the fluorescence variation—it may be any function of frequency, but we assume constancy in the spatial direction. However, this is not sufficiently accurate and false spectral features appear in the transmission. For example, note that division does not in fact remove the observed carbon and oxygen K edges that appear in both the unattenuated and attenuated backlight spectra. The carbon K-edge absorption, Fig. 3, is thus considered an experimental artifact and not representative of the bulk of the sample. The reason for this conclusion is that the observed K-edge absorption is representative of near-neutral carbon and this would not be the case if the carbon were integral to the BN sample.

The inaccuracy of the intensity calibration of the plate is also largest in the low exposure regime. Thus, we find that the regions of highest absorption are the most inaccurate in the current experiment. This effect is made all the worse by the fact that we were limited to relatively long backlight durations [18]. The long duration implies that the results may be compromised by the questionable backlight stability and other time-dependent effects.

We identify the duration and spatial uniformity of the backlight as areas that require much future effort. The deleterious effects of spatial nonuniformity will to some extent be ameliorated by shortening the time over which the absorption spectrum is recorded. This can be achieved by using a large-area backlight and gating the detector. In this way the uniformity must only be maintained for the gated duration. This would also reduce the background signal, which at present is integrated over the total duration of the experiment.

The resolving power of the instrument plays a critical role in the interpretation of large optical depth transitions. The saturated lines would provide critical information were it not for the instrumental broadening. In this case the loss is important because we cannot extract the information on the most highly populated states that have the largest absorption.

Finally, the characterization of the heating flux is performed in supporting experiments but is not performed in the absorption experiment itself. It is just this use of an x-ray heat source that allows us to isolate our study from the rather complex physics of the heating of matter by visible laser deposition, at the cost of a separate suite of characterization experiments. We have performed a number of series of measurements on the flux, and found in the more recent series larger integrated fluxes, by a factor of 1.5, than those measured in the original series. This casts doubt on the absolute flux found in the original measurements. The more recent measurements have been quite reproducible, which supports the validity of these data taken with newly calibrated instrumentation. We further note that the relative spectral content for the earlier and the more recent data is the same, so that it is the difference in the absolute flux level not the spectral shape that concerns us. The original data were possibly flawed by the following earlier systematic problems: lack of calibration of the phase plate transmission, inaccurate conversion calibration of the 1.053 to 0.52 μm laser light, Au target batch nonuniformity, or variations in the laser near-field beam profile. All of these possible sources of error are now checked on each experiment. Thus, the baseline flux data are the spectral data of the later Ref. [10]; we note, as mentioned previously, that this amounts to taking the spectral data of Ref. [9] and multiplying by 1.5.

B. Theory and simulation

The simulation of the experiment is on the whole quite successful. The main features of the experiment are reproduced and the obvious weaknesses of the atomic model do not in any significant way affect this conclusion. It is interesting to note that although the current ALTAIR atomic description does not contain easily observable features such as ionization potential depression (IPD) or detailed spectral line shapes intrinsic to the radiation-transfer calculations, the data reduction is not compromised. On the one hand, the IPD can be readily estimated and its effects are simply calculated so that the reduction can be checked in the observation. Other than the fact that the spectrum has an abrupt unphysical appearance, the IPD is not important in the interpretation of the data.

In contrast, the Stark spectral line shapes can be important in the detailed analysis of individual line profiles. However, given the spatial gradients and the integration time it is unproductive to attempt a meaningful Stark profile analysis. This shortcoming is easily overcome by the equivalent width analysis, which is much better suited to the data than any detailed line-shape analysis could be. Although the equivalent width provides important insights into the experimental design and the quality of the data, the line profile synthesis remains useful for identification purposes. Thus, the satellite spectra require a detailed approach for two complementary reasons. First, in the plasma the sum of the spectral contributions that arise from forbidden lines becomes substantial for non-hydrogenic systems at high enough electron density

to cause mixing of the dipole-allowed and forbidden components. The contributions of the forbidden components are derived from calculations of the spectral line profile emitted by the ion in the plasma environment. Second, the overlapping nature of the various satellite line transitions can be correctly calculated only when the manifold of interacting states is included. Thus, the placement and intensity of the components, once the Stark effect becomes important, can be studied only with an appropriate line-shape calculation.

The attenuation of the incident x-ray flux through the sample, and the impact this has on the electron temperature distribution, require detailed atomic data, for example, the front-to-back temperature asymmetry discussed above, where the differences between calculations "bnfs" and "bnla" can be ascribed to the x-ray absorption cross sections used during the respective hydrodynamic calculations. The increased accuracy provided by the present atomic model changes the predicted plasma conditions. This observation leads to the interesting possibility that the ionization balance is indeed the critical parameter for estimating the state of the sample, and will, when used together with other diagnostic information, provide a critical measure of the x-ray flux.

The need for spectroscopically accurate data for these low-Z elements has been discussed and the satellites for nitrogen are compiled. The situation for the boron satellites is less well defined at present. While it is obvious that additional effort could improve the set of energies for the appropriate boron satellites, as was done for the nitrogen satellites, the conclusions of the extended analysis would not significantly change. The path for compiling a sufficient data set is clear; however, the details would not have an effect on the conclusions we can draw. The important point to be gained from the analysis performed here is as follows: even for a rather spectrally coarse method such as equivalent width analysis, the spectral identification must be spectroscopically accurate.

In the analysis of the data the most fruitful method was found to be the equivalent widths of the K-shell lines and their associated satellites. It is from this analysis that we are able to make the most important conclusions. In brief summary we find that: (1) the equivalent width analysis can be used to bracket the ionization balance of the species from hydrogenic through berylliumlike, (2) the data for the heliumlike resonance line clearly indicates that in the data reduction residual background has not been extracted, and (3) the single representative temperature-density point used to generate the equivalent widths does not provide a consistent agreement with the simulated spectrum.

The results of the present analysis show that although we can perform the detailed simulations of the experiment, the observation can only be understood by independent analysis coupled to simpler models than are inherent in the complete radiation-hydrodynamics simulations. We note that it is not the object of the present analysis to attempt to get the simulation to fit the data. There are, of course, enough uncertainties to obtain a fit if we allowed the various aspects of the modeling to be free of constraint. Indeed, in using a multiplier greater than 1.5 we show that the x-ray flux will change the results, but that these do not bring us closer into agreement with the ionization balance or the measured spectrum. What we have learned is the limits of the techniques available. Thus, the simulated temperature seems somewhat low from the analysis of the experiment and this implies that there is in reality, a higher x-ray flux on the sample. However, a straight increase in flux does not resolve the problems. This therefore is a major issue for future work.

In summary, we have provided detailed analysis of an x-ray-heated, untamped, low-atomic-number sample and found broad agreement between simulation and experiment. In addition, we have gained sufficient information to allow the critical redesign of the experiment which will improve the data quality and quantity in future experiments.

ACKNOWLEDGMENTS

The initial measurements of the x-ray flux were in large part carried out in a series of experiments performed by D. R. Kania with support from H. N. Kornblum. The advice and assistance of L. B. Da Silva and B. J. MacGowan on the fielding of experiments in the Nova two-beam facility are greatly appreciated. We have had several useful discussions with C. A. Iglesias about the interpretation of the BN spectrum, and have benefited from comparisons with Iglesias's and F. J. Rogers's LTE opacity code OPAL. We would like to recognize the assistance we have received on the atomic models from K. T. Cheng and J. H. Scofield, and especially K. T. Chung and U. I. Safronova, who provided some very valuable satellite line data for nitrogen. This work was performed under the auspices of the U.S. Department of Energy by Lawrence Livermore National Laboratory under Contract No. W-7405-ENG-48.

APPENDIX A: PLATE CALIBRATION PROCEDURE

The calibration of the plates used in the experiment, Kodak 101-5, has not been documented in the spectral range of interest to this experiment. There exist calibrations for the closely related 101-7 plates, which have a monolayer of AgBr grains [19]. The 101-5 plates, in addition to the AgBr, have a gel coating that is composed of an unspecified thickness of carbon and oxygen. Further, the entire set of experimental data is taken at grazing incidence angles from roughly 4.87° to 7.87°, where the previous data are limited. These considerations led to the calibration of the plates.

To achieve the calibration the following had to be done. First, a model of the intensity onto the emulsion had to be formulated. We assume that a source that has a well-characterized temperature—and therefore has a blackbody distribution—produces the incident intensity. The source must then be reflected by the gold mirror and diffracted by the grating. At this point the source im-

pinges on the gel coating that covers the emulsion. The blackbody distribution is assumed known, and the responses of the Au mirror and the grating as a function of frequency (or wavelength) are known from independent measurement.

With this approach the response of the plate to an intensity can be quantified and thus reduced to a fixed relation between exposure and intensity. The analysis of the measurements performed in this way contains two free parameters. First we assume that the intensity source has a temperature of 200 eV, which is found *a posteriori* to be satisfactory. The second parameter is the thickness of the gel coating. We assume that the gel has an areal density of 1×10^{25} cm^{-2} made up of C and O atoms that form a layer 300 Å thick. This thickness gives calculated C and O absorption features that are in good agreement with the observed features in the unfiltered spectrum, and therefore we assume that this is a reasonable value. Thus the largest error remains the initial source intensity, and using a Planck distribution at 200 eV proves to give the best relative fit across the entire spectral region of interest.

In Fig. 14 we show some of the experimental data taken at wavelengths ranging from 25 to 66 Å. The data presented have been reduced by removing the angular dependence from the intensity versus plate density relationship given in Ref. [19], Eq. (8), as

$$D = a\,[1 - \exp(-bI \sin\theta)] \ , \qquad \text{(A1)}$$

where I is the intensity, θ is the grazing angle, D is the exposed plate density, and a and b are fitting constants. Our calibration data are fitted using the values $a = 2.0$ and $b = 0.313$. In Fig. 14 the fit given by Eq. (A1) for these parameters is shown together with the data. We note that these parameters are close to those determined by Henke, but that the $\sin\theta$ factor is important in obtaining the correct fit. The inaccuracy of the fit for low exposure levels is sufficient in itself to explain the deviations between theory and experiment for those spectral regions where the absorption is large.

APPENDIX B: SATELLITE LINE DATA

The first step in this search was the work of Gabriel [16] and Vainshtein and Safronova (VS) [17]. The notation of Li-like $1s2\ell2\ell'$ satellites follows Gabriel. In Table III we give the line positions for these satellites in N according to MCDF, Refs. [16] and [17], and others to be discussed below. The most glaring problem with the "bnla" spectrum in this region (cf. Fig. 12) is that the three multiplets jkl, a–d, and qr are all blended near 420 eV, while the experimental spectrum shows two blends, one near 419-eV, and one near 421 eV. From Gabriel's data, and also Vainshtein's and Safronova's, it is clear that the 419-eV blend is jkl, and the 421-eV blend is the combination of a–d and qr. The two evident features near 426–427 eV in the experimental spectrum do not line up well with the "bnla" lines, but they do agree with st and mn in the Vainshtein and Safronova [17] data set. The statement in Vainshtein and Safronova that Gabriel's data should be preferred for $Z < 10$ is not supported by this BN spectrum.

In the course of this work we were able to get a new set of calculations of Li-like N from Professor Safronova [20]. These are shown in Table III under the heading "S94." Through the kindness of Professor K. T. Chung of North Carolina State University [21] we were also able to get still another set of calculations of the $1s2p2\ell$ doublet satellites in Li-like N; these are given in Table III. The three computational approaches used by Gabriel (Vainshtein and), Safronova, and Chung are somewhat different. Gabriel's method uses the nonrelativistic Hartree-Fock method followed by a diagonalization of the intermediate-coupling Hamiltonian. Vainshtein and Safronova use a $1/Z$-expansion method to express the Hamiltonian as a polynomial in Z, the diagonalization of which gives the energy levels. Neither of these approaches is well suited to N V, since this is a few-electron system that is still dominated by electron correlations, and therefore configuration interaction is significant. Chung uses a variational configuration interaction

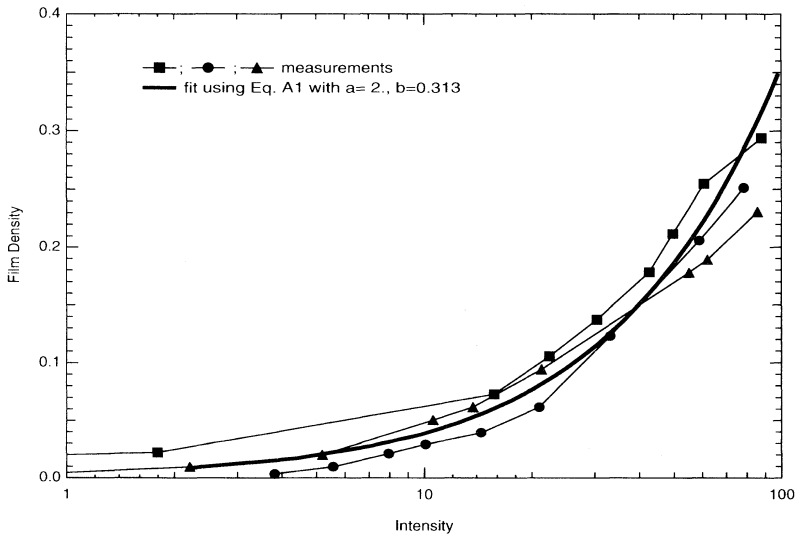

FIG. 14. Experimental plate density-exposure relations at three wavelengths, shown by the light curves connecting the squares, triangles, and circles, compared with the fit given by Eq. (A1), shown by the solid curve. The intensity is in arbitrary, but constant, units.

TABLE III. Transition energies in eV for $1s^2 2\ell$–$1s2p2\ell$ satellite lines in N V.

Key letter	Multiplet	MCDF	Gabriel [16]	Vainshtein and Safronova [17]	Safronova [20]	Chung [21]
abcd	$1s^2 2p\ ^2P^o$-$1s2p^2\ ^2P$	420.31	420.71	420.39	420.32	420.82
e–i	$1s^2 2p\ ^2P^o$-$1s2p^2\ ^4P$	414.36	415.08		415.01	
jkℓ	$1s^2 2p\ ^2P^o$-$1s2p^2\ ^2D$	419.59	419.29	419.14	419.06	419.29
mn	$1s^2 2p\ ^2P^o$-$1s2p^2\ ^2S$	427.70	427.24	426.70	426.63	426.75
op	$1s^2 2p\ ^2P^o$-$1s2s^2\ ^2S$	399.41	401.24	400.59	400.51	
qr	$1s^2 2s\ ^2S$-$1s2p(^1P)2s\ ^2P^o$	419.83	421.57	421.19	421.10	421.33
st	$1s^2 2s\ ^2S$-$1s2p(^3P)2s\ ^2P^o$	425.71	425.77	425.33	425.25	425.40
uv	$1s^2 2s\ ^2S$-$1s2p(^3P)2s\ ^4P^o$	412.98	413.97	414.02	413.93	
w	$1s^2\ ^1S$-$1s2p\ ^1P^o$	430.70	430.65	430.70	430.59	
xy	$1s^2\ ^1S$-$1s2p\ ^3P^o$	426.30	426.21	426.49	426.37	

method with a very large basis set for the nonrelativistic part of the calculation [22,23]; this should be a good technique for N V. Chung estimates that the accuracy of his energy levels, apart from the more approximate autoionization shifts and QED corrections, is substantially better than 0.1 eV.

Safronova's transition energies [20] are seen to agree well with the Vainshtein and Safronova (VS) set [17], as might be expected since the same method was used. Chung's energies lie generally intermediate between those of Gabriel and VS, perhaps a little closer to the latter. The large value for *a–d* and the relatively small values of *st* and especially of *mn* produce a satellite line pattern for Chung's calculations that gives the best agreement of all the calculations with the experimental spectrum.

The most prominent of the Be-like N satellites should be the set $1s^2 2\ell 2\ell'$-$1s2p2\ell 2\ell'$. Our data for these were also given to us in a private communication from Professor Safronova; the relevant excited-state term-average energies are listed in Table IV. We used the laboratory values of the singly excited-state energies in N IV as much as possible to derive the wavelengths. The original data, and our calculations, use the wavelengths for individual lines, not multiplets, but the multiplet members cannot be resolved at the resolution of our spectra.

There are no definitely identified lines of Be-like N in the experimental spectrum at or near the wavelengths derived from Table IV. The noise level in the spectrum can be used to set upper limits to the equivalent widths of these lines. These are discussed in Sec. V A.

Li-like B satellite lines are seen in the experimental spectrum. The line positions used for these in the ALTAIR "bnla" calculation are listed in the column headed MCDF in Table V. The energies derived from Ref. [17] are also listed in Table V. The differences are more than 2 eV in some cases. The experimental spectrum has features at 197.83, 198.28, 199.21, and 202.74 eV. The first three might be identified as *jkℓ*, *abcd*, and *qr*, respectively, based on VS. The identity of the line at 202.74 is uncertain; if this is *st*, then a blip at 204.59, in the wing of the He-like resonance line (205.56), might be *mn*. A more accurate calculation of the satellite energies is clearly needed, but this is not available at present.

This work has not so far extended to a consideration of the $1s2p3\ell$ and $1s2p2\ell 3\ell'$ Li-like and Be-like satellites of He-like Lyman β. Some of the necessary data are given in Ref. [24]. A number of these Li-like satellites are visible in our spectrum in the range 474–493 eV. (These

TABLE IV. Energy levels in eV for $1s2p2\ell 2\ell'$ satellites in N IV.

Key	term	Safronova [20]
I33	$1s2s^2 2p\ ^3P^o$	410.58
K53	$1s2s(^3S)2p^2\ ^5P$	413.19
I13	$1s2s^2 2p\ ^1P^o$	414.14
Q33	$1s2s(^1S)2p^2\ ^3P$	420.92
K35	$1s2s(^3S)2p^2\ ^3D$	421.41
K15	$1s2s(^1S)2p^2\ ^1D$	426.71
K31	$1s2s(^3S)2p^2\ ^3S$	426.16
J51	$1s2p^3\ ^5S$	428.59
K33	$1s2s(^3S)2p^2\ ^3P$	428.17
K11	$1s2s(^1S)2p^2\ ^1S$	431.46
K13	$1s2s(^3S)2p^2\ ^1P$	430.60
J35	$1s2p^3\ ^3D^o$	433.11
J31	$1s2p^3\ ^3S^o$	434.31
J15	$1s2p^3\ ^1D^o$	435.98
J33	$1s2p^3\ ^3P^o$	437.64
J13	$1s2p^3\ ^1P^o$	440.55

TABLE V. Transition energies in eV for $1s^2 2\ell$–$1s2p2\ell$ satellite lines in B III.

Key letter	Multiplet	MCDF	Vainshtein and Safronova [17
abcd	$1s^2 2p\ ^2P^o$-$1s2p^2\ ^2P$	199.99	198.52
jkℓ	$1s^2 2p\ ^2P^o$-$1s2p^2\ ^2D$	199.88	197.96
mn	$1s^2 2p\ ^2P^o$-$1s2p^2\ ^2S$	205.30	202.91
op	$1s^2 2p\ ^2P^o$-$1s2s^2\ ^2S$	186.62	186.14
qr	$1s^2 2s\ ^2S$-$1s2p(^1P)2s\ ^2P^o$	199.08	198.87
st	$1s^2 2s\ ^2S$-$1s2p(^3P)2s\ ^2P^o$	203.61	201.84
w	$1s^2\ ^1S$-$1s2p\ ^1P^o$	205.57	205.46
xy	$1s^2\ ^1S$-$1s2p\ ^3P^o$	202.95	203.10

states also contribute weaker satellites of Lyman α, quite close in energy to the resonance line, as discussed in Ref. [25]. In the present case, since we observe the lines in absorption, the strength of the lines with the additional 3ℓ spectator electron is down by the population ratio, e.g., $N(1s^2\,3\ell)/N(1s^2)$. This ratio is of order 0.05 for nitrogen, which explains why these lines are too weak to be separated from the resonance lines in our spectra.)

[1] J. M. Foster *et al.*, Phys. Rev. Lett. **67**, 3255 (1991); T. S. Perry *et al.*, *ibid.* **67**, 3784 (1991); L. B. Da Silva *et al.*, Phys. Rev. Lett. **69**, 438 (1992).

[2] J. Koch *et al.*, J. Quant. Spectrosc. Radiat. Transfer **54**, 227 (1995); J. C. Moreno, C. A. Back, R. C. Cauble, J. A. Koch, and R. W. Lee, Phys. Rev. E **51**, 4897 (1995).

[3] A. Calisti, F. Khelfaoui, R. Stamm, B. Talin, and R. W. Lee, Phys. Rev. A **42**, 5433 (1990).

[4] B. A. Hammel *et al.*, Europhys. Lett. **20**, 319 (1992); B. A. Hammel *et al.*, in *Radiative Properties of Hot Dense Matter*, edited by W. Goldstein, C. Hooper, J. Gautier, J. Seely, and R. Lee (World Scientific, Singapore, 1992), p. 22.

[5] J. F. Seely *et al.*, J. Quant. Spectrosc. Radiat. Transfer **51**, 349 (1994).

[6] As described by D. Del Giudice and C. Colmenares (private communication), Auger electron spectroscopy was used to analyze the composition of a similar sample foil both before and after sputtering off a surface layer contaminated with C and O. Before sputtering the composition was B: 54%, N: 14%, C: 24%, and O: 8%; after sputtering it became B: 85%, N: 13%, C: 0%, and O: 2%.

[7] W. E. Behring *et al.*, Appl. Opt., **27**, 2762 (1988).

[8] J. I. Castor, P. G. Dykema, and R. I. Klein, Astrophys. J. **387**, 561 (1992).

[9] D. R. Kania *et al.*, Phys. Rev. A **46**, 7853 (1992).

[10] C. A. Back *et al.*, J. Quant. Spectrosc. Radiat. Transfer **51**, 19 (1994).

[11] J. K. Nash, D. C. Eder, and H. A. Scott, in *Ultrashort-Wavelength Lasers*, edited by S. Suckewer, SPIE Proceedings No. 1551 (Society for Photo-Optical Engineers, Bellingham, 1992), Sec. 2, p. 79.

[12] I. P. Grant, B. J. McKenzie, P. H. Norrington, D. F. Mayers, and N. C. Pyper, Comput. Phys. Commun. **21**, 207 (1980); B. J. McKenzie *et al.*, *ibid.* **23**, 233 (1980).

[13] J. H. Scofield, Lawrence Livermore National Laboratory Report No. UCRL-51326 (unpublished).

[14] M. H. Chen, Phys. Rev. A **31**, 1449 (1985).

[15] S. Bashkin and J. O. Stoner, Jr. *Atomic Energy Levels and Grotrian Diagrams. Volume I. Hydrogen I - Phosphorus XV* (North-Holland, Amsterdam, 1975).

[16] A. H. Gabriel, Mon. Not. R. Astron. Soc. **160**, 99 (1972).

[17] L. A. Vainshtein and U. I. Safronova, At. Data Nucl. Data Tables **21**, 49 (1978).

[18] On the Nova two-beam facility the pulse lengths for the beams must be identical.

[19] B. L. Henke, S. L. Kwok, J. Y. Uejio, H. T. Yamada, and G. C. Young, J. Opt. Soc. Am. B **1**, 818 (1984).

[20] U. I. Safronova (private communication). We are grateful to Professor Safronova for these results, and to Dr. J. Nilsen for making our need known to her.

[21] K. T. Chung (private communication).

[22] B. F. Davis and K. T. Chung, Phys. Rev. A **37**, 111 (1988).

[23] B. F. Davis and K. T. Chung, Phys. Rev. A **39**, 3942 (1989).

[24] L. A. Vainshtein and U. I. Safronova, At. Data Nucl. Data Tables **25**, 311 (1980).

[25] P. Wang, J. J. MacFarlane, and G. A. Moses, Phys. Rev. E **48**, 3934 (1993).

[26] G. B. Zimmerman and W. L. Kruer, Comments Plasma Phys. Cont. Fus. **2**, 51 (1975).

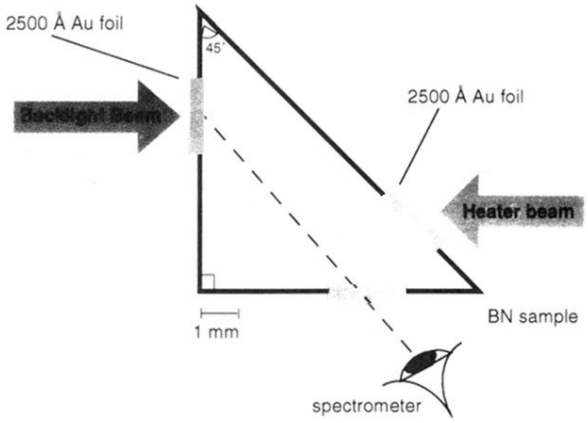

FIG. 1. The experimental arrangement. The triangular structure is a hollow copper prism into which three windows are machined where stainless steel washers are mounted. The BN sample is mounted on one of these washers, and gold foils are mounted on the other two. The beams of the Nova two-beam facility are focused on the gold foils. The spectrometer line of sight is directed through the sample foil at the backlight foil, as shown.

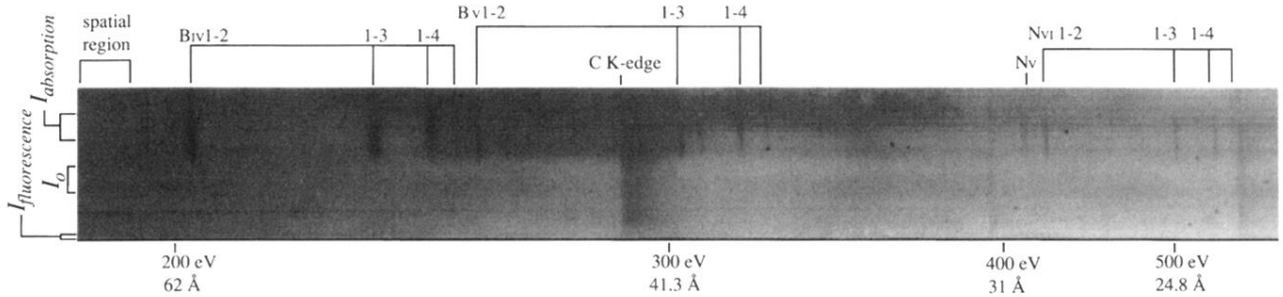

FIG. 2. The plate record obtained in the experiment. The annotations show the wavelength and photon energy scales and the areas used for the backlight and absorption spectra and the fluorescence signal estimate.